Journal of Applied Electrochemistry (2006) 36:441–448
DOI 10.1007/s10800-005-9095-6

Mechanism of di(methyl)ether (DME) electrooxidation at platinum electrodes in acid medium

G. KÉRANGUÉVEN, C. COUTANCEAU*, E. SIBERT, F. HAHN, J- M. LÉGER and C. LAMY
UMR-CNRS 6503, Université de Poitiers, Equipe Electrocatalyse, 40 avenue du Recteur Pineau, 86022, Poitiers cedex, France
*(*author for correspondence, tel: +33-5-49-45-48-95, fax: +33-5-49-45-35-80, e-mail: christophe.coutanceau@univ-poitiers.fr)*

Received 28 February 2005; accepted in revised form 31 October 2005

Key words: dimethylether, electrooxidation, fuel cell, *in situ* Infrared Reflectance Spectroscopy, platinum

Abstract

The electrooxidation of DME was studied at a bulk platinum electrode. It was shown that the DME adsorption was a slow step in the overall oxidation reaction. The DME adsorption is potential dependent in the hydrogen region of platinum and independent in the double layer region. From low potential scan rate voltammetry and DME stripping experiments, it was shown that the DME oxidation mechanism occurred via several reaction paths. At low potentials, DME oxidation leads to the existence of a positive current plateau. ''In situ'' Infrared Reflectance Spectroscopy experiments were carried out to identify the intermediate and reaction products of DME adsorption and oxidation at different potentials. CO_L (linearly bonded CO), CO_B (bridge bonded CO), adsorbed COOH species and CO_2 were detected. From these electrochemical and spectro-electrochemical results, it was proposed that some adsorbed DME was hydrolysed and directly oxidized to CO_2 or HCOOH species and some partially blocked platinum sites at the surface forming Pt–CHO and/or Pt–CO. Then, as soon as platinum becomes able to activate water, a bifunctionnal mechanism occurs to form either HCOOH or CO_2 again following two different reaction paths.

1. Introduction

Because of the difficulty of handling and storing hydrogen, many research agencies tend to develop fuel cells with the direct combustion of liquid fuels: the drastic decrease in the overall mass energy density when hydrogen is stored (Table 1) makes the use of liquid fuels such as alcohols very promising. Methanol and ethanol are the most studied fuels. With methanol, which only contains one carbon atom, power densities close to 180–200 mW cm^{-2} can be achieved at 90 °C [1–4], which makes methanol a good alternative liquid fuel to hydrogen in terms of electrical performance. But, because of its high toxicity, methanol is not a good candidate, particularly for automobile applications. Other alcohols are envisaged and studied for this purpose. Ethanol is of course the most studied [5, 6], because it is the simplest alcohol after methanol; it has little toxicity and can be produced from biomass, whereas methanol is produced from natural gas. Another alternative fuel for direct fuel cell applications is DME (dimethylether, also called methoxy methane) [7–10]. This compound, which has no C–C bond to break, has a good theoretical energy density of 8.2 kWh kg^{-1}, which is higher than that of methanol and close to that of ethanol (Table 1). Moreover, according to the thermodynamic data of DME combustion with oxygen ($\Delta G_{reac} = -1362$ kJ mol^{-1}) [7], the standard reversible cell voltage related to the following equation (1) is 1.18 V:

$$CH_3{-}O{-}CH_3 + 3H_2O \rightarrow 2CO_2 + 12H^+ + 12e^- \quad (1)$$

$$3O_2 + 12H^+ + 12e^- \rightarrow 6H_2O \quad (2)$$

$$CH_3{-}O{-}CH_3 + 3O_2 \rightarrow 2CO_2 + 3H_2O \quad (3)$$

with a total number of exchanged electrons of 12, as for the electrooxidation of ethanol. DME is also an interesting compound for fuel cell applications because of its physical properties: it is a gas at room temperature, but its boiling point is only −23 °C and liquid phase storage as for LPG is easy. It can also be used as a liquid fuel because of its solubility in water close to 76 g l^{-1} (i.e. 1.65 mol l^{-1}) at 20 °C under a pressure of 1 bar [8]. This solubility corresponds to the concentration ranges generally used in a Direct Methanol Fuel Cell [11–13] or a Direct Ethanol Fuel Cell (DMFC) [5, 14, 15].

Table 1. Theoretical mass energy density of different fuels

Fuels	Energy densities/kWh kg^{-1}
H_2	32.8
H_2 in a 200 bar pressurized tank (1.5% wt. storage)	0.42
CH_3OH	6.1
CH_3OCH_3	**8.2**
CH_3CH_2OH	8.0

In the present work we present some electrochemical results on the electrooxidation of DME at a bulk platinum electrode in order to obtain kinetic data. Then, fuel cell experiments and *in situ* IR reflectance spectroscopy measurements are carried out in order to evaluate the behaviour of this fuel at platinum electrodes in terms of reactivity and to determine the distribution of reaction intermediates and products. From the results a mechanism is proposed which is more complex than those presented earlier [7–10].

1.1. *Electrochemical measurements*

The electrochemical set-up consisted of a Voltalab PGZ 402 potentiostat controlled by a computer. The electrolytic solutions were prepared from 96% H_2SO_4 (Suprapur, Merck) in ultra-pure water (MilliQ, Millipore, 18 MΩ cm). The electrochemical experiments were carried out at 20 °C using a conventional thermostated three-electrode electrochemical cell. The desired concentrations of DME in the electrolyte were obtained by addition of a given volume of a saturated DME solution in a known volume of the N_2-purged solution in the cell. The working electrode was a platinum sphere (0.14 cm diameter, 0.062 cm^2 geometric surface area), the counter electrode was a platinum grid and the reference electrode was a mercury mercurous sulphate electrode (MSE), but all potentials are related to the Reversible Hydrogen Electrode (RHE).

1.2. *Fuel cell tests*

The Membrane Electrode Assemblies (MEAs) were prepared, by hot pressing at 130 °C for 90 s under a pressure of 35 kg cm^{-2}, a pretreated Nafion®117 membrane with E-TEK electrodes (2.0 mg cm^{-2} Pt loading, 40% metal/C, 40% PTFE, 0.8 mg cm^{-2} Nafion®).

The fuel cell tests in a single cell with a 5 cm^2 geometric surface area were carried out with a Globe Tech test bench. The E vs. j and P vs. j curves were recorded using a high power potentiostat (Wenking model HP 88) interfaced with a PC to apply constant current sequences and to store the data, and a variable resistance in order to fix the current applied to the cell.

Generally, fuel cell tests are carried out with gaseous DME hydrated by bubbling in hot water at temperatures close to 80 °C before feeding the anodic compartment of the cell [7, 9, 10]. Because the management of a liquid fuel is easier than that of a gaseous fuel (in term of storage), a saturated solution of DME in water at 20 °C was used to feed the anodic compartment. The DME concentration of a saturated solution is 1.65 M [8].

1.3. In situ *infrared reflectance spectroscopy measurements*

A Bruker IFS 66v FTIR spectrometer was modified for beam reflection on the electrode surface at a 65° incident angle. To remove interferences from atmospheric water and CO_2 the beam path was vacuum evacuated. An Infrared Associates liquid nitrogen-cooled HgCdTe detector was used. Spectral resolution was 4 cm^{-1}.

The infrared cell was equipped with a CaF_2 window and a working electrode fixed to a glass rod fitted through the top of the cell (permitting it to be pressed against the CaF_2 window) [16]. The working electrode consisted of a platinum disk (diameter 8 mm) glued to a glass tube as holder. A Pt wire was used as the counter electrode and a RHE was used as reference. The cell potential was controlled using an LB 81 Wenking potentiostat and a Hi-Tek waveform generator connected to a Kip and Zonen BD 90 XY recorder.

The electrode reflectivity was recorded each 30 s at a given potential. Each spectrum resulted from the co-addition of 128 interferograms. Final spectra were normalized as difference reflectivity change:

$$-\Delta A = \left(\frac{\Delta R}{R}\right) = \left(\frac{R_t - R_{t_0}}{R_{t_0}}\right)$$

where R_t is the reflectivity taken at time t and R_{t0} the reflectivity recorded at $t = 0$.

In this case a negative peak means the production of species and a positive band indicates the consumption of species at the electrode surface.

2. Results and discussion

2.1. *DME electrooxidation at a bulk Pt electrode*

Figure 1 presents the voltammograms of a platinum sphere recorded in 0.1 M H_2SO_4 electrolyte with and without 0.1 M DME. The voltammograms are in good agreement with those obtained under the same experimental conditions by Müller et al. [8]. In the low potential range, the hydrogen adsorption–desorption region of the platinum electrode is greatly disturbed by the presence of DME. Oxidation waves starting at potentials close to 0.65 V vs. RHE and reaching a maximum current at a potential close to 0.78 V vs. RHE appeared. For potentials higher than 0.9 V vs. RHE, the j(E) polarisation curves in the presence and absence of DME are not superimposed, which indicates that some adsorbed species are present at the platinum surface and blocks the formation of surface oxides. This is confirmed

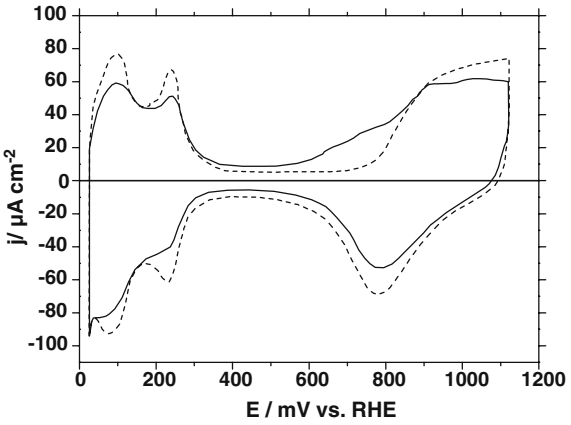

Fig. 1. Cyclic voltammograms of a Pt sphere electrode recorded in 0.1 M H_2SO_4 at 20 °C, v = 50 mV s^{-1}, (- - -) without DME, (—) with 0.1 M DME.

in the negative potential scan, where a lower charge density is involved in the reduction peak of the platinum oxides in the presence of DME.

Adsorbed OH species are formed on the platinum surface in the range 0.45–0.75 V vs. RHE [17]. These species are likely involved in the electrooxidation of DME into CO_2 and/or formic acid (HCOOH) according to the bi-functional mechanism [18, 19], since both products were detected by other authors in the anode outlet of a direct DME fuel cell [7, 8]. For higher potentials platinum tends to be recovered by oxide species and it seems that DME does not adsorb or react at these oxide species. In the presence of DME the voltammogramm of platinum in the potential range 0.3–0.65 V vs. RHE is slightly shifted positively, which indicates that DME undergoes oxidation in this potential range.

The decrease in current in the hydrogen adsorption–desorption region of platinum indicates that DME adsorbs at a platinum surface. Figure 2 represents the I/v curves recorded at platinum in a 0.1 M H_2SO_4 + 0.6 M DME solution for different scan rates.

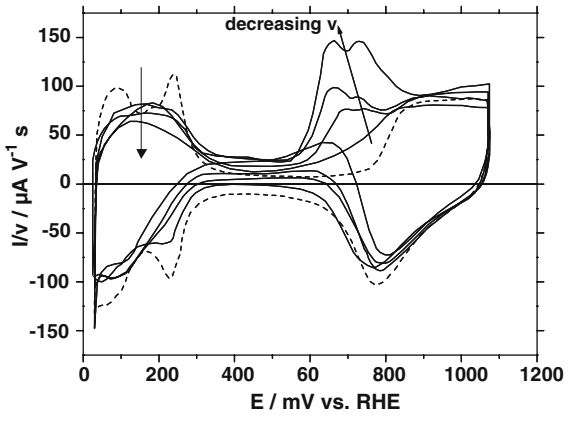

Fig. 2. I/v vs. E curves of a Pt sphere electrode recorded in 0.1 M H_2SO_4 (- - -) and in 0.1 M H_2SO_4 + 0.6 M DME electrolyte at 20 °C (—), v = 10, 20, 50 and 100 mV s^{-1}.

For each voltammogram the current was divided by the corresponding scan rate in order to determine the contribution of DME adsorption kinetics in the limiting process. For the voltammograms recorded at low potential scan rates (10 and 20 mV s^{-1}) an oxidation plateau between 0.3 and 0.65 V vs. RHE is clearly marked. The current of this plateau is not a capacitive one but a faradaic one as it is the same in the positive and negative potential scans, confirming that DME is partially oxidised at relatively low potentials on platinum. Increase in scan rate leads to a decrease in the maximum current of the DME oxidation peaks (expressed in μA V^{-1} s). These oxidation peaks are likely due to adsorbed species which react with adsorbed OH species at platinum. On the other hand one may expect, in the case of a reaction controlled by an adsorption step, that the value of the maximum current of the oxidation peaks divided by the corresponding scan rate value remains constant. But, in this region, the whole oxidation reaction of DME involves the adsorption of at least two species (adsorbed CO species and adsorbed OH species) and is complex. However, it seems that the adsorption step of DME is likely limiting in the DME oxidation process. DME adsorption at platinum being slow, no peak appears for a potential scan rate of 100 mV s^{-1}, only an oxidation wave from 0.55 to 0.9 V vs. RHE.

Another interesting point is the appearance of two oxidation peaks for low potential scan rates. These two oxidation peaks are well defined at 10 mV s^{-1}, but the relative intensity of the second peak, i.e. the peak located at higher potentials, compared to that of the first peak tends to decrease with increase in the potential scan rate. It becomes a shoulder at 50 mV s^{-1} and disappears at higher scan rates (100 mV s^{-1} for example). This fact indicates that either different platinum sites have to be considered for DME oxidation, or that different DME oxidation mechanisms take place.

Because the adsorption of DME at platinum is a slow process the platinum sphere was held for 10 min at a given potential (from 0.1 to 0.6 V vs. RHE) prior to voltammetric experiments in order to facilitate the DME adsorption [8]. The oxidation peaks were integrated in order to determine the quantity of electricity (Q_{ox}) involved. According to the IR reflectance spectroscopy measurements discussed later (part 3.3), one may assume that these peaks are due to the oxidation of adsorbed CO species. Therefore, Q_{ox} is directly related to the coverage of platinum by adsorbed species (θ_{org}) and its determination allows characterisation of the activity of platinum towards the DME adsorption process as a function of potential (Figure 3). For adsorption potentials in the range 0.1–0.2 V vs. RHE, i.e. in the hydrogen region, adsorption appears to be potential dependent since Q_{ox} increases with increasing adsorption potential. For potentials from 0.2 to 0.55 V vs. RHE (i.e. in the region where either hydrogen adsorbs weakly or no species are adsorbed), the adsorption of DME appears to be potential independent since

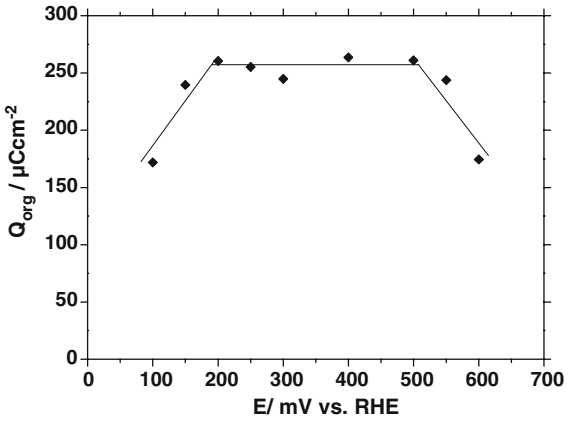

Fig. 3. Superficial charge Q_{ox} associated with DME oxidation recorded at a Pt sphere electrode in 0.1 M H_2SO_4 electrolyte containing 0.6 M DME at 20 °C and $v = 20$ mV s^{-1} plotted as a function of the adsorption potential.

Q_{ox} is constant with increasing adsorption potential, giving an average value of 260 μC cm^{-2} (geometric surface area). For potentials higher than 0.55 V vs. RHE, Q_{ox} decreases because of the formation of OH species at the surface leading to the oxidation of adsorbed species from DME. This indicates, in agreement with the results obtained by other authors [8], that DME adsorption at platinum is not favoured in comparison with other adsorbed species (hydrogen, hydroxyls or oxides). The variation in coverage by adsorbed species coming from DME as a function of potential is comparable to that observed with methanol at platinum electrodes [20, 21].

DME stripping experiments are useful to obtain other interesting results concerning the DME adsorption at platinum (Figure 4). In the stripping experiment, DME is first adsorbed at the platinum sphere at 0.25 V vs. RHE for 10 min, then DME is removed from the solution by bubbling pure N_2 for 30 min, the platinum sphere remaining under potential control at 0.25 V vs. RHE. Then the potential sweep (20 mV s^{-1}) is started and voltammograms are recorded. In the first voltammetric cycle, the positive potential scan leads to the formation of an oxidation peak starting at 0.6 V vs. RHE. The maximum current is obtained at 0.8 V vs. RHE. This oxidation peak at 0.8 V vs. RHE is likely related to the second peak observed during DME electrooxidation experiments, which was located at potentials close to 0.75 V vs. RHE. Therefore, this second peak results from the oxidation of adsorbed species coming from DME. This peak involves a charge $Q_{org} = 295\,\mu$C cm^{-2} (geometric surface area), whereas the calculation from the charge involved in the adsorption region of hydrogen in the absence of DME gives $Q_H^0 = 310\,\mu$C cm^{-2} (geometric surface area), which corresponds to an electrode roughness factor close to 1.5, assuming a value of 210 μC cm^{-2} of true surface area for the formation of a monolayer of adsorbed H [22]. A quantity of electricity $Q_H = 48\,\mu$C cm^{-2}, corresponding to free Pt sites, is observed when the organic species coming from DME are adsorbed at the platinum electrode. The number of electron exchanged per adsorption site (N_{eps}) of species coming from DME can be evaluated as follows [23]:

$$N_{eps} = \frac{Q_{org}}{Q_H^0 - Q_H} \approx 1.13$$

The value of N_{eps} close to 1 and the IR measurements (see nest section) indicate that the main adsorbed species coming from DME adsorption at platinum is bridge bonded CO, even if several percent of the surface is recovered by linearly bonded CO. It can be assumed that a C-adsorption of DME occurs involving three adjacent platinum sites to break the three C–H bonds, as for methanol adsorption [24]. The adsorbed species resulting from the dissociative adsorption process involves two platinum sites. Indeed, assuming that 420 μC cm^{-2} of true surface area are involved to oxidize one monolayer of linearly adsorbed CO, the calculation of the degree of coverage of the platinum surface would give $\theta_{CO_L} \approx 0.47$, whereas the coverage by adsorbed species calculated from the hydrogen adsorption region gives $\theta_{org} = \frac{Q_H^0 - Q_H}{Q_H^0} \approx 0.84$. Therefore, bridge bonded CO seems to be formed at the platinum surface.

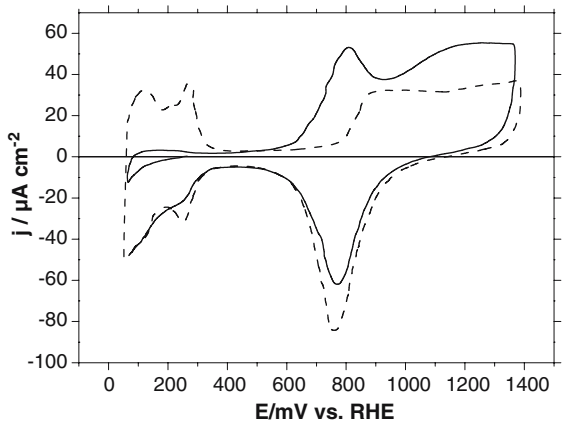

Fig. 4. Cyclic voltammograms of a Pt sphere electrode recorded in 0.1 M H_2SO_4 electrolyte at 20 °C, $v = 20$ mV s^{-1} without DME (—). First cycle of the stripping of a saturated layer of DME adsorption species recorded in 0.1 M H_2SO_4 electrolyte at 20 °C, $v = 20$ mV s^{-1} (- - -). DME was adsorbed from a 0.6 M solution at 0.25 V vs. RHE and 20 °C for 10 mn and removed from the solution by bubbling nitrogen for one hour with the electrode being under potential control.

2.2. *Direct DME fuel cell tests*

The maximum current of oxidation at 50 mV s^{-1} obtained at platinum in a 0.1 M DME solution is close to 15 μA cm^{-2}. This value is very low compared to that obtained under the same conditions in a 0.1 M MeOH solution, which typically reaches 2–3 mA cm^{-2}, i.e. two orders of magnitude higher [21]. Müller et al. [25] have already observed this behaviour by comparing cyclic

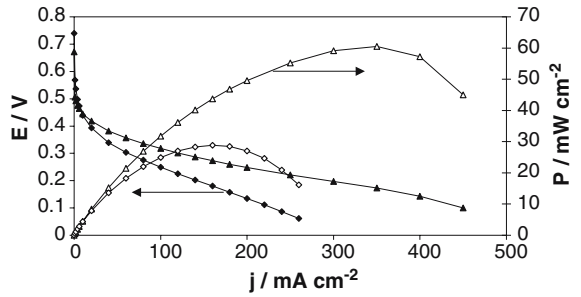

Fig. 5. $E(j)$ and $P(j)$ curves recorded in a 5 cm^2 single Direct DME Fuel cell working at 90 °C : ◆,◇ 1.65 M DME, ▲,△ 2.0 M MeOH. P_{O2} = 3 bar, P_{DME} = P_{MeOH} = 2 bar.

voltammetry of MeOH and DME oxidation at platinum electrodes. However, electrooxidation experiments of DME and MeOH in a 5 cm^2 fuel cell under stationary conditions indicates that the reactivity of DME in terms of maximum power density is half that of methanol, being 30 and 60 mW cm^{-2}, respectively. The activation energy for each oxidation processes is certainly different, but this result was rather unexpected because of the very low reactivity of DME at room temperature. The $E(j)$ polarisation curves obtained at 90 °C with a Pt/C catalyst at the anode are represented in Figure 5. The open circuit voltage (OCV) in the Direct DME Fuel cell close to 0.75 V is in agreement with that obtained by other authors at platinum or platinum-ruthenium electrodes with hydrated gaseous DME [8–10]. This open circuit voltage is higher than that obtained with methanol (0.68 V), indicating that either cross-over of DME or poisoning of the catalyst are lower with this fuel.

2.3. *Discussion on the electrooxidation mechanism of DME*

Two mechanisms of DME electrooxidation at platinum or platinum-ruthenium catalysts have been reported in previous work [8, 9]. For Müller et al. [8], the first steps of DME oxidation consists in a C-adsorption of DME at a platinum site followed by hydrolysis of the adsorbed molecules into Pt–CHO species and methanol, according to the following equations:

$$\mathrm{Pt} + \mathrm{CH_3{-}O{-}CH_3} + \mathrm{H_2O} \rightarrow \mathrm{Pt{-}CHO} + \mathrm{CH_3OH} + 3\mathrm{H^+} + 3\mathrm{e^-} \quad (4)$$

Then,

$$\mathrm{Pt{-}CHO} \rightarrow \mathrm{Pt{-}CO} + \mathrm{H^+} + \mathrm{e^-} \quad (5)$$

$$\mathrm{Pt} + \mathrm{H_2O} \rightarrow \mathrm{Pt{-}OH} + \mathrm{H^+} + \mathrm{e^-} \quad (6)$$

$$\mathrm{Pt{-}CO} + \mathrm{Pt{-}OH} \rightarrow \mathrm{Pt} + \mathrm{CO_2} + \mathrm{H^+} + \mathrm{e^-} \quad (7)$$

In parallel, oxidation to CO_2 of methanol formed in reaction (3) occurs via the well known bi-functional mechanism [18, 26], via a 6-electron process. This mechanism leads only to the formation of CO_2 as product. It cannot explain the two observed peaks in the electrochemical experiments. Moreover, Tsutsumi et al. [9] have analysed the reaction products formed in the anode compartment of a direct DME Fuel cell. They did not detect methanol and formaldehyde, but formic acid (HCOOH). On the basis of these results, they proposed a different mechanism. In this mechanism, the adsorption of DME took place via 2 platinum sites for each carbon of the DME molecule to form a $Pt_2{-}COH{-}HOC{-}Pt_2$ species, which would give $2Pt_3{-}COH$ after reacting with one water molecule, following by the formation of two $Pt_2{-}CO$ species after the intervention of two more water molecules. From this latter species, two reaction paths could occur: either the formation of HCOOH after reacting with one water molecule (this complete reaction path involving 8 electrons) or the formation of adsorbed OH species and reaction between the CO_{ads} species and the OH_{ads} species to produce CO_2 (this complete reaction path involving 12 electrons). This mechanism of DME electrooxidation may explain the appearance of the two oxidation peaks. If one assumes that the kinetics of HCOOH formation is higher than that of the CO_2 formation, then the oxidation peak at low potentials can be due to the reaction path leading to HCOOH and the second one to the reaction path leading to CO_2. But, the production of formic acid, HCOOH, at platinum catalyst is expected at low potentials, i.e. potentials lower than 0.3 V vs. RHE, whereas at higher potentials, this species becomes very electro-reactive [27] and it is likely that it reacts at platinum to form CO_2. Moreover, according to the values of the maximum current attributed to the oxidation of adsorbed CO species in the DME electrooxidation experiments and to that obtained from the DME stripping, it seems that this oxidation peak is only due to the reaction of adsorbed species, i.e. no turnover of DME at the platinum sites occurs. On the other hand, the relatively good performance in fuel cell experiments indicates that DME turnover occurs at platinum catalysts. According to our knowledge $Pt_3{-}COH$ species have never been detected by spectrochemical techniques.

According to Müller et al. [25], the voltammograms of DME oxidation tend to superimpose to that of methanol oxidation after several voltammetric cycles. They conclude that, in acid medium, DME undergoes hydrolysis to form methanol. This fact is in agreement with our DME adsorption results, which showed the same dependence of Q_{org} on potential as methanol. The fuel cell results also indicate that, in the super acid environment of the Nafion membrane, DME could be hydrolysed partially to methanol, hence enhancing the fuel cell performance. The relatively high open circuit voltage in Fuel Cell experiments and the existence of the oxidation plateau in low potential scan rate experiments indicate that DME oxidation takes place at low potentials. This is confirmed by *in situ* IR reflectance experiments at low

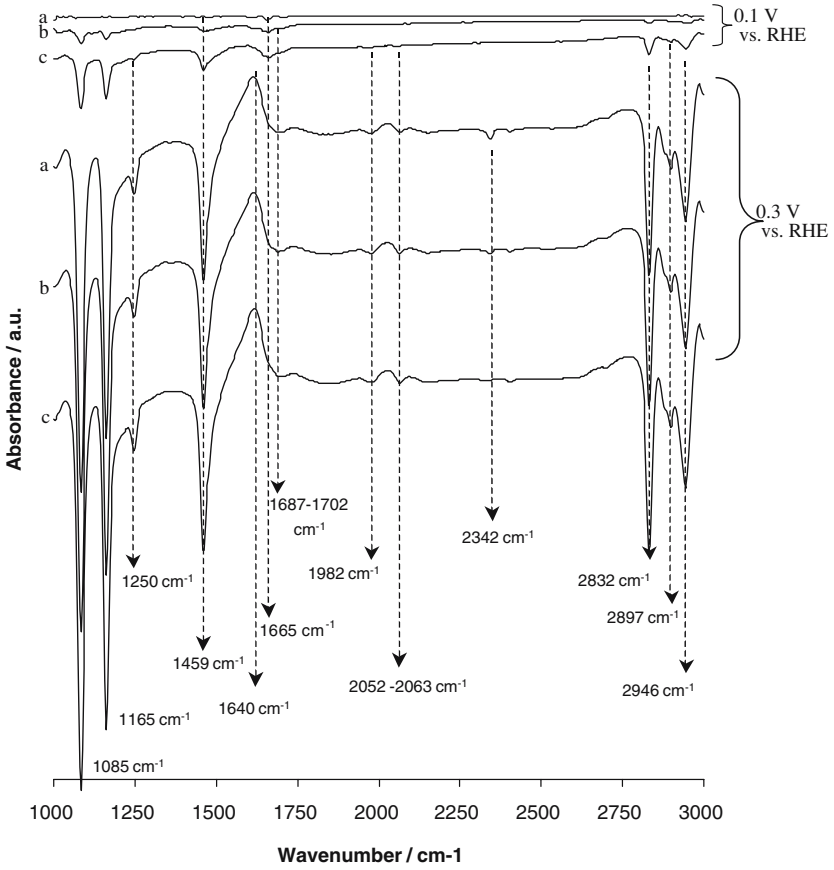

Fig. 6. IR reflectance spectra of the DME adsorption at a Pt electrode as a function of time for two adsorption potentials (100 and 300 mV vs. RHE) recorded at 20 °C. (a) after 30 s; (b) after 280 s; (c) after 780 s.

potentials, i.e. an adsorption study of DME at potentials of 0.1 and 0.3 V vs. RHE as a function of time (Figure 6). At 0.1 V vs. RHE, negative absorption bands appear located at wavenumbers close to 1085, 1165, 1250, 1459, 1665, 1687, 2832, 2897 and 2946 cm^{-1} and a positive one located at 1640 cm^{-1}, and after 780 s two bands appear located at 1982 and 2052 cm^{-1}. A negative band is due to the formation of adsorbed species or species at the vicinity of the electrode surface, whereas a positive band is due to consumption of adsorbed species or species close to the electrode surface. After 780 s these bands clearly indicate the formation of bridge-bonded CO_B (close to 1950 cm^{-1}) and linearly bonded CO_L (close to 2050 cm^{-1}) [28–30], with slow kinetics and low platinum surface coverage at this potential as suggested by the DME adsorption experiments. The absorption band located at 1982 cm^{-1} confirms the presence of bridge bonded CO, which was considered from the N_{eps} calculation in the previous part. The absorption band located close to 1640 cm^{-1} can be attributed to the in-plane deformation vibration of interfacial water [31]. The bands located close to 1085 and 1165 cm^{-1} are difficult to assign. In this wavenumber region the IR spectra may be affected by the presence of absorption bands due to SO_4^{2-} and HSO_4^- [32], but they can also be attributed to ν(C–O–C) and r(CH_3) vibration modes of DME [33, 34]. Therefore, no indication can be drawn from these bands. The absorption band located close to 1250 and 1480 cm^{-1} were also assigned by Asselin et al. [33] and Schriver-Mazzuoli et al. [34] to the r(CH_3) and δ(CH_3) vibration modes of DME. The absorption band close to 1700 cm^{-1} was assigned to ν_{CO} of COOH or CHO [35–37]. These bands can be correlated with those appearing close to 2844, 2900 and 2950 cm^{-1} which can be assigned to (CH) from $HCOO_{ads}$ or CH_3OH_{ads} [38]. Therefore, it can be proposed that adsorbed HCOO exists at the electrode surface. At 300 mV vs. RHE the same bands are present, but with higher intensity, indicating that reaction occurs (water consumption and formation of products). The absorption band close to 1687 cm^{-1} at 0.1 V vs. RHE is shifted towards higher wavenumber (close to 1702 cm^{-1}) indicating the existence of adsorbed HCOO species. A shift in the frequency of an absorption band is characteristic of an adsorbed species and can be explained either by the Stark effect, which is observed only for adsorbed species for which the location of the absorption band is potential dependent [28], or by a change in species coverage, or by a difference in the Pt-adsorbate bond strength, as suggested by Rice et al. [39] for adsorbed CO. At the same time three other bands exist, located close to 1982, 2052–2063 and 2342 cm^{-1}. At this potential the formation of bridge-bonded CO_B (close to 1950 cm^{-1}) and linearly bonded CO_L (close to

2050 cm^{-1}) [28–30] also occurs at the electrode surface but with higher kinetics and leading to higher coverage. Moreover, the formation of CO_2 (absorption band close to 2340 cm^{-1}) was unexpected at such low potentials (close to 0.3 V vs. RHE).

Therefore, another mechanism can be proposed where the adsorption of DME blocks a part of the platinum surface area (about 85%, as shown by DME stripping experiments) at low potentials according to the earlier proposed mechanism, leaving the other part of the platinum surface area free for direct DME oxidation. In this mechanism, one has to take into account the formation of methanol, formic acid and CO_2 at low potentials, and the formation of linearly and bridge-bonded CO species. In the low potential range, the direct oxidation of DME giving a current plateau can occur via C-adsorption and hydrolysis of the molecule:

$$CH_3{-}O{-}CH_3 + H_2O \rightarrow CH_2OH_{ads} + CH_3OH + H^+ + e^- \quad (8)$$

and/or

$$CH_3{-}O{-}CH_3 + H_2O \rightarrow 2CH_2OH_{ads} + 2H^+ + 2e^- \quad (8')$$

followed by:

$$CH_2OH_{ads} \rightarrow CHO_{ads} + 2H^+ + 2e^- \quad (9)$$

then,

$$CHO_{ads} + H_2O \rightarrow CO_2 + 3H^+ + 3e^- \quad (10)$$

and/or

$$CHO_{ads} + H_2O \rightarrow HCOOH + H^+ + e^- \quad (10')$$

and/or

$$CHO_{ads} \rightarrow CO_{ads} + H^+ + e^- \quad (10'')$$

This mechanism, which involves the intervention of several non activated water molecules, is likely governed by very slow kinetics and may explain the very low values of current at the oxidation plateau in the low potential range. For higher potentials (higher than 0.55 V vs. RHE), platinum becomes able to activate water and to adsorb OH species:

$$H_2O \rightarrow OH_{ads} + H^+ + e^- \quad (11)$$

then, two reactions can take place:

$$CHO_{ads} + OH_{ads} \rightarrow CO_2 + 2H^+ + 2e^- \quad \text{(first peak)} \quad (12)$$

and,

$$CO_{ads} + OH_{ads} \rightarrow CO_2 + H^+ + e^- \quad \text{(second peak)} \quad (13)$$

To confirm these assumptions more detailed *in situ* IR spectroscopic measurements and analysis of the distribution of reaction products as a function of the electrode potential is necessary, in order to determine the reaction products as well as the adsorbed intermediates.

3. Conclusion

DME adsorption is a slow step in DME oxidation at platinum. This adsorption process is potential dependent at low potentials and becomes potential independent from 0.2 to 0.55 V vs. RHE. DME oxidation seems to take place following at least three different paths – leading to HCOOH or CO_2 via (Eq. 10 and 10′, respectively), to CO_2 via either (Eq. 12) or Eq. (13) – as demonstrated by the existence of two oxidation peaks and of a positive current plateau. *In situ* IR reflectance spectroscopy identified some intermediates and reaction products of DME adsorption and electrooxidation at platinum: CO_L (linearly bonded CO), CO_B (bridge-bonded CO), adsorbed COOH species and CO_2. The electrochemical, spectroelectrochemical and fuel cell experiments suggest a complex mechanism for DME electrooxidation.

References

1. A.K. Shukla, C.L. Jackson, K. Scott and R.K. Raman, *Electrochim. Acta* **47** (2002) 3401.
2. A.S. Aricò, V. Baglio, E. Modica, A. Di Blasi and V. Antonucci, *Electrochem. Comm.* **6** (2004) 164.
3. R. Dillon, S. Srinivasan, A.S. Aricò and V. Antonucci, *J. Power Sources* **127** (2004) 112.
4. V. Gogel, T. Frey, Zhu Yongsheng, K.A. Friedrich, L. Jörissen and J. Garche, *J. Power Sources* **127** (2004) 172.
5. F. Vigier, C. Coutanceau, A. Perrard, E.M. Belgsir and C. Lamy, *J. Appl. Electrochem.* **34** (2004) 439.
6. F. Vigier, C. Coutanceau, F. Hahn, E.M. Belgsir and C. Lamy, *J. Electroanal. Chem.* **563** (2004) 81.
7. Y. Tsutsumi, T. Moriyama and S. Kajitani, in V. W. Wong (MIT) (Ed.), Proceeding of the 2000 Spring Technical Conference of The ASME Internal Combustion Engine Division, ICE Vol. 34–3 (2000), pp 58–63.
8. J.T. Müller, P.M. Urban, W.F. Hölderich, K.M. Colbow, J. Zhang and D.P. Wilkinson, *J. Electrochem. Soc.* **147** (2000) 4058.
9. Y. Tsutsumi, Y. Nakano, S. Kajitani and S. Yamasita, *Electrochemistry* **70** (2002) 984.
10. M.M. Mench, H.M. Chance and C.Y. Wang, *J. Electrochem. Soc.* **151** (2004) A144.
11. A.S. Aricò, P. Cretì, E. Modica, G. Monforte, V. Baglio and V. Antonucci, *Electrochim. Acta.* **45** (2000) 4319.
12. C. Coutanceau, A.F. Rakotondrainibe, A. Lima, E. Garnier, S. Pronier, J.-M. Léger and C. Lamy, *J. Appl. Electrochem.* **34** (2004) 61.
13. Y.J. Kim, W.C. Choi, S.I. Woo and W.H. Hong, *Electrochim. Acta* **49** (2004) 3227.
14. W.J. Zhou, Z.H. Zhou, S.Q. Song, W.Z. Li, G.Q. Sun, P. Tsiakaras and Q. Xin, *Appl. Catal. B: Environ.* **46** (2003) 273.
15. W.J. Zhou, W.Z. Li, S.Q. Song, Z.H. Zhou, L.H. Jiang, G.Q. Sun, Q. Xin, K. Poulianitis, S. Kontou and P. Tsiakaras, *J. Power Sources* **131** (2004) 217.
16. A. Bewick, K. Kunimatsu, B. Pons, J.W. Pons and J.W. Russell, *J. Electroanal. Chem.* **160** (1984) 47.
17. T. Iwasita, *Electrochim. Acta* **47** (2002) 3663.
18. M. Watanabe and S. Motoo, *J. Electroanal. Chem.* **60** (1975) 275.

19. H.A. Gasteiger, N. Markovic, P.N. Ross and E.J. Cairns, *J. Electrochem. Soc.* **141** (1994) 1795.
20. B.J. Piersma and E. Gileadi. in JO'M. Bockris (Ed.), Modern Aspects of Electrochemistry, Vol. 4, Ch. 2., (Butterworths, London, 1966), pp. 102.
21. J.-M. Léger, PhD thesis (University of Poitiers, France, 1982).
22. C. Coutanceau, M.J. Croissant, T. Napporn and C. Lamy, *Electrochim. Acta* **46** (2000) 579.
23. A. Papoutsis, J.M. Léger and C. Lamy, *J. Electroanal. Chem.* **234** (1987) 315.
24. A. Kabbabi, R. Faure, R. Durand, B. Beden, F. Hahn, J.-M. Léger and C. Lamy, *J. Electroanal. Chem.* **444** (1998) 41.
25. J.Müller, P. Urban, R. Wezel, K.M. Colbow and J. Zhang, US Patent no US 6,777,116 B1, Aug. 17. 2004.
26. P. Waszczuk, A. Wieckowski, P. Zelenay, S. Gottesfeld, C. Coutanceau, J.-M. Léger and C. Lamy, *J. Electroanal. Chem.* **511** (2001) 55.
27. W.T. Napporn, H. Laborde, J.-M. Léger and C. Lamy, *J. Electroanal. Chem.* **404** (1996) 153.
28. B. Beden, C. Lamy, A. Bewick and K. Kunimatsu, *J. Electroanal. Chem.* **121** (1981) 343.
29. K. Kunimatsu, *J. Electroanal. Chem.* **140** (1982) 205.
30. B. Beden, F. Hahn, S. Juanto, C. Lamy and J.-M. Léger, *J. Electroanal. Chem.* 225 (1987).
31. B. Rasch and T. Iwasita, *Electrochim. Acta* **35** (1990) 989.
32. M. El Chbihi, D. Takky, F. Hahn, H. Huser, J.-M. Léger and C. Lamy, *J. Electroanal. Chem.* **463** (1999) 63.
33. P. Asselin, P. Soulard, M.E. Alikhani and J.P. Perchard, *Chem. Phys.* **249** (1999) 73.
34. L. Schriver-Mazzuoli, J.M. Coanga, A. Schriver and P. Ehrenfreund, *Vibrational Spectro* **30** (2002) 245.
35. T. Iwasita and E. Pastor, *Electrochim. Acta* **39** (1994) 531.
36. S.C. Chang, L.W. Leung and M.J. Weaver, *J. Phys. Chem.* **94** (1990) 6013.
37. T. Iwasita, B. Rasch, E. Cattaneo and W. Vielstich, *Electrochim. Acta* **34** (1989) 1073.
38. C. Lamy, A. Lima, V. LeRhun, F. Delime, C. Coutanceau and J.-M. Léger, *J. Power Sources* **105** (2002) 283.
39. C. Rice, Y.Y. Tong, E. Oldfield, A. Wieckowski, F. Hahn, F. Gloaguen, J.-M. Léger and C. Lamy, *J. Phys. Chem. B* **104** (2000) 5803.